C. R. Palevol 16 (2017) 545–556

Contents lists available at ScienceDirect

Comptes Rendus Palevol

www.sciencedirect.com

Human Palaeontology and Prehistory (Palaeoanthropology)

Assessing cranial plasticity in humans: The impact of artificial deformation on masticatory and basicranial structures

Évaluer la plasticité crânienne chez l'Homme : impact des déformations artificielles sur les structures masticatrices et basicrâniennes

Marion Cottin [a], Roman Hossein Khonsari [b], Martin Friess [a,*]

[a] *UMR 7206, département "Homme et Environnement", Muséum national d'histoire naturelle, Musée de l'Homme, 75016 Paris, France*
[b] *Service de chirurgie maxillofaciale et stomatologie, Assistance publique–Hôpitaux de Paris, hôpital universitaire Pitié-Salpêtrière, université Pierre-et-Marie-Curie, 75013 Paris, France*

ARTICLE INFO

Article history:
Received 29 July 2016
Accepted after revision 8 March 2017
Available online 16 May 2017

Handled by Roberto Macchiarelli and Clément Zanolli

Keywords:
Artificial cranial deformation
Basicranial flexion
Temporomandibular joint
Covariation
Geometric morphometrics

ABSTRACT

Artificial cranial deformations (ACD) are a widespread cultural practice found in numerous historical and prehistoric contexts. Their study can yield valuable insight into craniofacial growth, specifically into the interactions between neurocranial and basicranial modules. This study seeks to reinvestigate the presumed effect of ACD on basicranial and masticatory elements by applying a 3D geometric morphometric approach to CT scans. A total of 51 French and Bolivian skulls, representing anteroposterior and circumferential deformations and including undeformed individuals, were scanned, and 3D landmarks were submitted to between-group principal components analysis and two-block partial least-squares analysis. Our results illustrate changes in basicranial shape and in cranial base angles induced by ACD, as well as in masticatory geometry, namely in the relative position of the mandibular fossae. Furthermore, our findings highlight differential effects of the various deformation types, which suggest that patterns of covariation between modified vaults and their associated basicrania are more complex than previously assumed, thereby stressing the degree of plasticity in human craniofacial growth.

Mots clés :
Déformation crânienne artificielle
Flexion basicrânienne
Articulation temporomandibulaire
Covariation
Morphométrie géométrique

RÉSUMÉ

Les déformations artificielles du crâne (DAC) désignent une pratique culturelle observée dans de nombreux contextes historiques et préhistoriques. Leur étude nous renseigne sur la croissance craniofaciale, notamment l'interaction entre les modules neuro- et basicrâniens. L'objectif de cette étude est de réexaminer l'effet présumé des DAC sur les éléments basicrâniens et masticateurs, en appliquant des méthodes de morphométrie géométrique 3D à des analyses tomodensitométriques. Au total, 51 crânes d'origine française et bolivienne, représentant les déformations antéropostérieures et circonférentielles, ainsi que des individus non déformés, ont été scannés, et les coordonnées de points de repère 3D ont été

* Corresponding author.
E-mail address: martin.friess@mnhn.fr (M. Friess).

http://dx.doi.org/10.1016/j.crpv.2017.03.001

étudiées par analyse en composantes principales intergroupes ainsi que par régression des moindres carrés partiels (PLS) avec deux blocs de covariation. Nos résultats illustrent des changements de conformation et d'angulation de la base du crâne, induits par les DAC, ainsi que de la géométrie masticatrice, notamment concernant les positions relatives de la fosse mandibulaire et du reste de la base du crâne. Nos observations soulignent des effets différentiels selon les types de déformation, ce qui suggère que les patrons de covariation entre une voûte modifiée et la base crânienne sont plus complexes que précédemment proposé.

1. Introduction

The custom of transforming the human body, be it for aesthetic motives or for the purpose of demonstrating membership to social or ethnic groups, has been omnipresent throughout human history and, in the case of artificial cranial deformations (ACD), can be traced back as far as the Palaeolithic period (Antón and Weinstein, 1999; Brown, 1981; Dingwall, 1931). Anthropologists continue to study deformations as a phenomenon at the interface between culture and biology that can inform on a variety of aspects regarding population history, craniofacial growth dynamics, but also respond to the very practical necessity to identify deformed skulls in collections or archaeological samples (Clark et al., 2007; Hoshower et al., 1995; O'Brien and Stanley, 2011; Tiesler, 2014; Torres-Rouff, 2002; Verano, 2003).

1.1. Deformational effects on the cranial base and face

From a morphological perspective, ACD can be seen as the outcome of a real-life experiment, albeit unplanned, on altering growth trajectories (Cheverud et al., 1992; Jimenez et al., 2012; Liebermann et al., 2000). As such, it has been used to investigate patterns of craniofacial variation in humans by looking at secondary effects of vault modifications induced on other structures, namely the face and the base. Previous studies have shown that, due to the morphological integration of the skull, deforming the braincase during extended periods of growth leads to changes in the cranial base and face. However, as it has been pointed out (Antón, 1989; Friess and Baylac, 2003), findings differ between studies, leaving some doubt as to the exact nature and patterns of some of these changes, and possibly reflecting uncertainties in the identification of deformation types. While the number and nomenclature of ACD vary according to different authors, a major distinction found in many publications is made between annular (or circumferential, C) and tabular (or anteroposterior, AP) types. This binary system is thought to reflect the two main types of deformation devices: soft wrapping vs. hard materials (tablets made from wood or stone). The use of these devices also tends to result in fundamentally different cranial shapes: C-type deformations lead to postero-superiorly protruding and mediolaterally narrow vaults, whereas the AP-type is characterized by anteroposteriorly shortened and mediolaterally widened braincases (Antón, 1989; Dembo and Imbelloni, 1938; Falkenburger, 1938). Within AP deformations, a subdivision into erect and oblique forms, though not supported by all scholars, has been proposed on the basis of the vertical/inclined orientation of the occipital squama (e.g., Dembo and Imbelloni, 1938).

In addition to the general change in neurocranial shape, various associated modifications in the face and base have been reported, though not all studies agree on all of these. Thus, several authors found facial broadening in AP-type deformations vs. narrowing in C-type deformations (Antón, 1989; Cheverud et al., 1992; Jimenez et al., 2012; Kohn et al., 1993). Increased facial height dimensions have also been reported in AP deformations (Antón, 1989), while some studies observed different degrees of facial shortening and flattening in AP (Cheverud et al., 1992; Jimenez et al., 2012).

With respect to the cranial base, the effects of the various deformation types have been estimated inconsistently: several studies (Antón, 1989; McNeill and Newton, 1965) found flattened basicrania (platybasia) in both AP- and C-type deformations, while others observed platybasia in C-, and basicranial kyphosis in AP-types (Martínez-Abadías et al., 2009; Moss, 1958). Furthermore, support for platybasia in AP also comes from Oetteking (1924), while Schendel et al. (1980) found no effect on the cranial base angle (CBA) at all. Conversely, the overall proportions of the cranial base, when investigated, have been consistently found altered depending on the deformation type: AP deformations result in anteroposteriorly shortened and mediolaterally widened basicrania, while C deformations yield the opposite shape, i.e., an anteroposteriorly lengthened and mediolaterally narrowed base (Antón, 1989; Cheverud et al., 1992; Cocilovo et al., 2011; Kohn et al., 1993; Martínez-Abadías et al., 2009).

Regarding the inconsistent findings with respect to CBA, previous studies have identified as potential causes differences in: (1) sample size, varying between $N = 65$ (Moss, 1958) and $N = 1586$ (Cocilovo et al., 2011); (2) classification of deformation types; (3) methodology (e.g., external vs. radiographic-based measurements, different definitions of CBA; see Antón, 1989; Cocilovo et al., 2011). However, differential effects on the base by deformation type have also been observed in studies with comparatively large sample sizes (e.g., Baylac and Friess, 2005; Martínez-Abadías et al., 2009) and, according to Antón (1989), differences in CBA definition do not account for these inconsistencies either. External vs. internal measurements (radiography, computed tomography) may also represent a potential cause for differences in the assessment of CBA.

The purpose of the present contribution is to compare the external and internal morphologies of deformed and undeformed skulls based on data obtained from standard medical imaging devices. This approach allowed us to address the following aspects quantitatively: 1) the effects of ACD on the skull base, specifically, the overall shape of the base as well as its angular variations; 2) the effects of ACD on the masticatory apparatus, specifically, the spatial relationship between the upper jaw and the mandibular fossa of the temporomandibular joint (TMJ).

2. Material and methods

The sample used in this study consists of 51 specimens from the anthropological collections of the "Muséum national d'histoire naturelle" (MNHN), Paris. Based on the fusion of the spheno-occipital synchondrosis and third molar (M3) eruption stage, they are all adult except two adolescent individuals. Due to incomplete information, sex was not used in subsequent analyses. The sample was recruited from two major geographic regions: South America and Europe. The South-American sample includes 39 individuals from Bolivia and has been collected by Georges de Créqui Monfort and Eugène Sénéchal de La Grange at the beginning of the 20th century (Chervin, 1908). It is mostly composed of two ensembles, one of which is an Aymara sample from Tiwanaku (or Tiahuanaco, Lake Titicaca), the other one being largely from Asnapujio in the South of the country (Chervin, 1908; Falkenburger, 1938). Based on the collectors' reports (Chervin, 1908; Créqui Monfort and Sénéchal de La Grange, 1904; Falkenburger, 1938), the Bolivian sample was generically attributable to the pre-Hispanic period. In the case of Tiwanaku, the remains are likely to date between the 4th and 11th centuries CE (Janusek, 2008), though a more refined chronometric dating has yet to be established.

The other geographic group consists of 12 French individuals, predominantly from the Southwest region: seven deformed skulls from the 19th century and five undeformed skulls from megalithic burials in Sauveterre (Manouvrier and De Mortillet, 1893).

The Bolivian skulls exhibit both anteroposterior and circumferential deformations, while the French skulls show a circumferential deformation known as the "Toulouse-type" (Broca, 1871; Dingwall, 1931). Toulouse-type deformations result from prolonged wearing of tightly wrapped head scarves known as "bandeau", and reports attest to the survival of this practice until the end of the 19th century (Broca, 1871). While it remains unclear to which extent head shape alteration was actually sought or merely an accepted side effect, both the resulting head shape and the mechanics used to achieve it match those of circumferential deformations known from other parts of the world, and thus warrant their inclusion in studies on the craniofacial effects of ACD. Still, because they stem from a different geographic and cultural context, for the purposes of this study they were considered as a separate group from the South-American C-type.

Undeformed skulls of both geographic regions were also included in the analyses. Identification of presence/absence and type of deformation were performed by one of us (MF).

Table 1
Sample composition by geographic origin and deformational status. ND: undeformed specimens; AP: anteroposterior (oblique/erect); C: circumferential crania; T: Toulouse-type deformation.
Tableau 1
Composition de l'échantillon par origine géographique et par type de déformation. ND : spécimens non déformés ; AP : déformation antéro-postérieure (oblique/droite) ; C : déformation circonférentielle ; T : déformation toulousaine.

Origin	ND	AP (o/e)	C	T	Total
Bolivia	10	19 (9/10)	10	–	39
France	5	–	–	7	12
Total	15	19	10	7	51

Given the difficulty to identify artificial deformations in cases of minimal alteration, specimen selection targeted clearly deformed skulls and presumably undeformed ones. Consequently, there was a higher chance for a minimally deformed skull to be misidentified as undeformed than vice versa. The assignment to C and AP-type, on the other hand, was further backed up by checking the cranial index (breadth/length), which is significantly higher in AP than in C deformations. Table 1 provides a summary of the sample composition.

All crania were scanned with a medical CT scanner using specific parameters for dry bone (Badawi-Fayad et al., 2005). The final voxel size was 0.45 mm × 0.45 mm × 0.4 mm. Each skull was segmented using a modified half-maximum height protocol (Fajardo et al., 2002; Spoor et al., 1993), and 3D landmark coordinates were extracted using Avizo 8.1 (FEI Inc, Hilsboro, OR). Repeatability was assessed by computing mean delta and standard deviations of a series of repeated landmark measurements and found to be below 1 mm, thus complying with osteometric standards (Bräuer, 1988; Buikstra and Ubelaker, 1994). The mandible, while highly informative for overall craniofacial and masticatory morphology, in particular, was not included in this study due to incomplete records and the uncertainty in achieving exact occlusion in the absence in several specimens of condyles and/or lower teeth.

Missing landmarks were estimated through thin-plate spline warping using the Morpho library for R (version 2.3.1.1; Schlager, 2016). The number of missing landmarks was below the recommended threshold of 20% (Couette and White, 2010) except for one case. Landmarks were then normalized via Generalized Procrustes Analysis (GPA; Rohlf, 2000) and subsequently submitted to multivariate statistics. Group-differences were tested with a between-group principal components analysis (PCA) and patterns of covariation between different cranial elements were investigated with two-block partial least-squares analysis (2B PLS; (Rohlf and Corti, 2000). Between-group PCA was based on the total set of landmarks, while 2B PLS used subsets of landmarks based on their assignment to the vault, cranial base, and masticatory apparatus.

Table 2 lists the landmarks and their assignment to cranial modules (Fig. 1). The choice of landmarks was mostly driven by our purposes, i.e., the need to capture the overall neuro- and basicranial shape, as well as the relative position of masticatory elements, such as the mandibular fossa,

Table 2
List of landmarks used in this study and their assignment to functional modules. Abridged definitions as per Martin (in Bräuer, 1988), unless specified.
Tableau 2
Liste des points de repère utilisés dans cette étude, ainsi que leur attribution à un module fonctionnel. Sauf mention particulière, les définitions abrégées suivent celles de Martin (dans Bräuer, 1988).

Landmark number	Name	Definition	Module
1	F. caecum	Center of the foramen caecum opening, mid-sagittal	Base
2	Posterior cribriform	Posterior margin of the cribriform plate, in the sagittal plane	Base
3	Jug. sphen.	Jugum sphenoidale	Base
4	Sella	Center of the sella turcica	Base
5, 6[a]	Lesser sphenoid	Most anterior point of the lesser sphenoid wing	Base
7, 8	Clinoid tip	Tip of the anterior clinoid process	Base
9, 10	Petrous tip	Most antero-medial point on the pars petrosa	Base
11, 12	Internal auditory	Center of the internal auditory meatus, in the plane of maximum circumference	Base
13, 14	Canalis caroticus	Center of the carotid canal, in the plane of maximum circumference	Base
15	Staphylion	Posterior nasal spine, tangent along the most anterior points of the posterior palatine border	Mast.
16	Prosthion	Most anterior point of the alveolar arch in midsagittal	Mast.
17	Nasion	Intersection of the frontonasal sutures and the sagittal plane	Mast.
18	Bregma	Intersection of coronal and sagittal sutures	Vault
19	Lambda	Intersection of sagittal and lambdoid sutures	Vault
20	Inion	Intersection of the superior nuchal lines and the external occipital protuberance, midsagittal	Vault
21	Opisthion	Posterior border of the foramen magnum	Base
22	Basion	anterior border of the foramen magnum	Base
23	Glabella	Most anterior point of the supraciliary arches, midsagittal	Vault
24, 25	Orbitale	Most inferior point on the orbital margin	Mst.
26, 27	Posterior palatine	Most anterior point of the posterior palatine border	Mast.
28, 29	Ektomolare	Midpoint above M2 on the alveolar arch	Mast.
30, 31	Porion	Most superior point of external auditory meatus	Vault
32, 33	Mastoideale	Most inferior point on the mastoid process	Vault
34, 35	Asterion	Intersection of lambdoid, parietomastoid, and occipitomastoid sutures	Vault
36, 37	Petrotympanic	Petrotympanic fissure	Vault
38, 39	Entoglenoid tip	Most inferior point of the entoglenoid process	Mast.
40, 41	Articular eminence	Most inferior point of the articular eminence of the Fossa mandibularis	Mast.
42, 43	Zygomaxillare	Lowest point of the zygomatico-maxillary suture on the inferior margin of the cheek	Mast.

[a] Two numbers indicate a bilaterally measured landmark; single-numbered landmarks are midsagittal.

the alveolar plane, and the origin of the *m. masseter*. The use of extremal landmarks, such as euryon and opisthocranion, to capture the chief dimensions of the vault, was abandoned due to poor repeatability.

The assignment to different cranial modules largely followed Bastir and Rosas (2005), Bookstein et al. (2003), Martínez-Abadías et al. (2009), and von Cramon-Taubadel (2011), and aimed at obtaining a comparable number of landmarks per module. However, in some cases, assignments vary by author, as it is the case for landmark selection. Notably, von Cramon-Taubadel (2011) defines the 'chondrocranium' as a module, rather than the base, and most landmarks assigned here to the base and included by von Cramon-Taubadel, such as opisthion, are part of her 'chondrocranium'; conversely, porion and mastoideale are here assigned to the vault, following von Cramon-Taubadel (2011), whereas Martínez-Abadías et al. (2009) assign both to the base.

We then performed analyses of covariation between the vault/base and vault/masticatory apparatus using a single GPA for the whole sample (Klingenberg and Marugán-Lobón, 2013). We also performed covariation analyses for each a priori group separately (AP, C, T, undeformed) and compared the angle of the first PLS vectors in order to assess whether patterns of within-group covariation were similar or different between groups (Klingenberg and Marugán-Lobón, 2013; Klingenberg and Zimmermann, 1992).

Shape changes associated with PLS axes were visualized by regressing Procrustes residuals onto axis scores and predicting coordinates for extreme values and group means. Shape differences between groups were visualized using mean group configurations. The CBA was defined as the angle formed by foramen caecum, sella and basion, and alternatively by nasion, sella, and basion. All statistics were computed in R (version 3.30, R Development Core Team, 2016) using dedicated libraries (Adams and Otarola-Castillo, 2013; Dryden, 2015; Schlager, 2016), except for angular comparisons of PLS axes, which were performed in MorphoJ 1.06 (Klingenberg, 2011).

3. Results

3.1. Shape differences between deformation types

The between-group PCA (Table 3, Fig. 2a) confirmed significant shape differences between all a priori groups ($P < 0.01$ for all comparisons after 9999 permutations), with the greatest group contrast (btwGrpPC 1, 56% of total between-group variance) between the two circumferential groups (C and T), on the one hand, and AP-deformed and undeformed skulls, on the other hand. The second axis (btwGrpPC 2, 37%) opposes undeformed and AP deformed skulls and T to C. In third axis (7%, not displayed), T-type deformations scatter at the positive end, while C and ND are at the negative end.

The distances between group means (Table 3) suggest that the greatest shape differences are those between undeformed skulls and C-type deformations, followed by

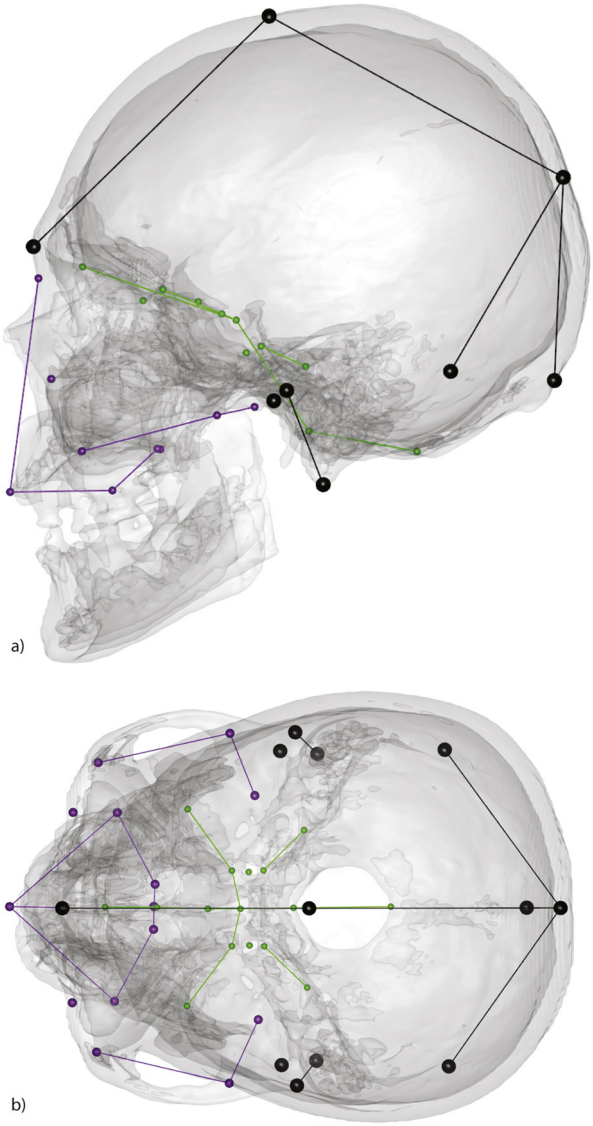

Fig. 1. Schematic representation of landmarks and their assignment to cranial modules in: (a) lateral and (b) superior views. Vault (black), cranial base (green), masticatory elements (purple).
Fig. 1. Représentation schématique des points de repère et de leur attribution à des modules crâniens en : (a) vue latérale et (b) vue supérieure. Voûte (noir), base crânienne (vert), éléments masticateurs (pourpre).

Table 3
Group differences: Euclidean distances between group means (above the diagonal) of the between-group PCA and *P*-values (below the diagonal) after 9999 permutations.
Tableau 3
Différences entre groupes : distances euclidiennes entre les moyennes des groupes (au-dessus de la diagonale) de l'ACP intergroupes et les valeurs *p* associées (en dessous de la diagonale) après 9999 permutations.

	AP	C	ND	T
AP	–	0.078	0.05	0.078
C	0.0001	–	0.084	0.064
ND	0.0001	0.0001	–	0.055
T	0.0001	0.0029	0.0077	–

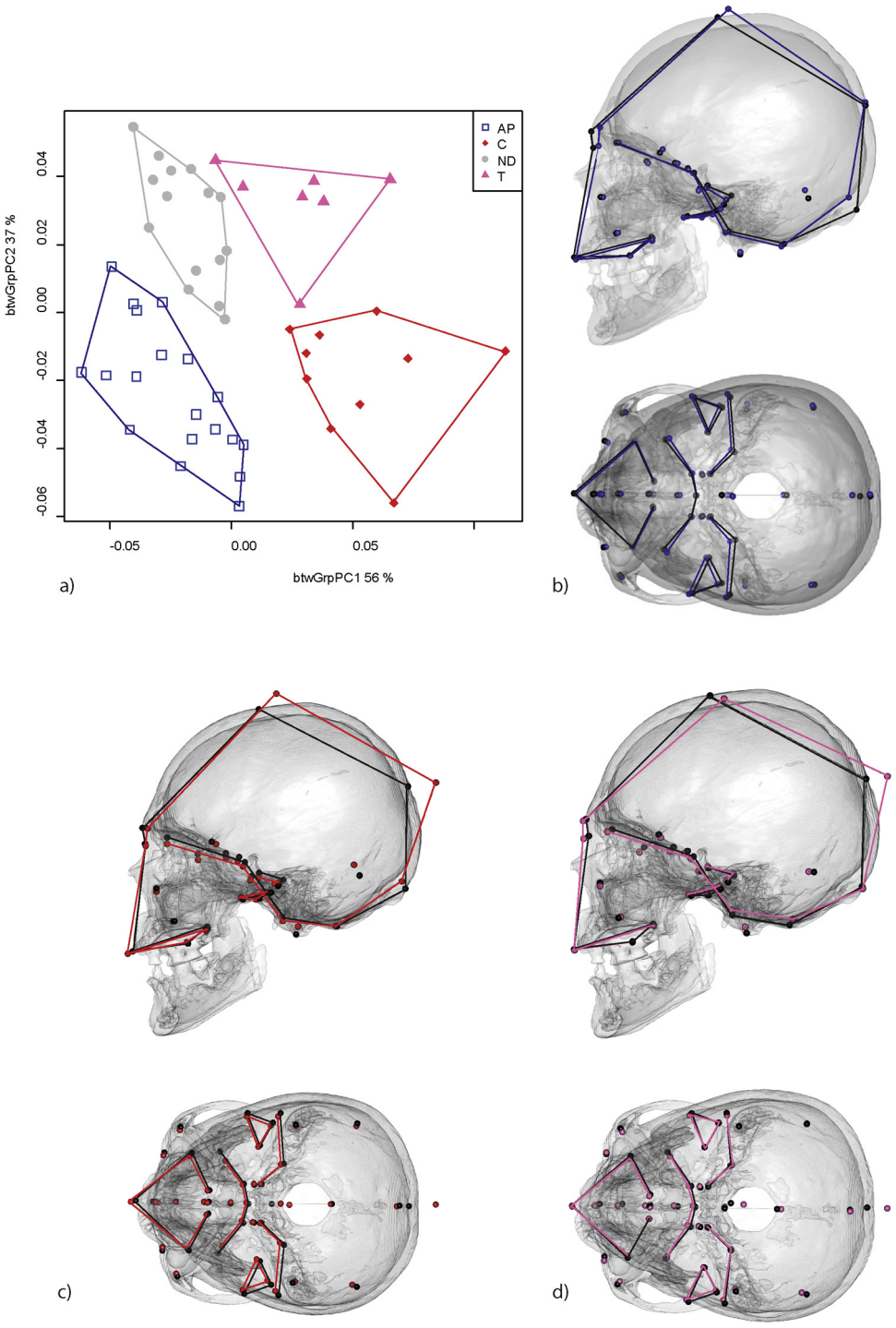

Fig. 2. Between-group PCA based on craniofacial landmarks (lateral and superior views). (a) Scatterplot of individual scores along PC1 (PC: principal component) and PC2, accounting for 93% of between-group variance. Associated shape differences between the mean undeformed configuration (ND, grey surface, black dots and lines) and the means of (b) the anteroposterior deformation (AP, blue dots and lines), (c) the circumferential deformation (C, red dots and lines), and (d) the Toulouse deformation (T, pink dots and lines).

Fig. 2. ACP intergroupes, basé sur des points de repère craniofaciaux (vues latérale et supérieure). (a) Nuage de points des scores individuels le long de CP1 (CP : composante principale) et CP2, expliquant 93 % de la variance intergroupe totale. Différences de conformations associées entre la configuration moyenne non déformée (ND, surface grise, points et polygones noirs) et la moyenne de (b) la déformation antéropostérieure (AP, points et polygones bleus), (c) la déformation circonférentielle (C, points et polygones rouges) et (d) la déformation toulousaine (T, points et polygones roses).

Table 4
Singular values and pairwise correlations of PLS scores between blocks: complete sample. RV-coefficient = 0.79, $P < 0.0001$ after 9999 permutations.
Tableau 4
Valeurs singulières et corrélations par paires de scores PLS entre blocs : échantillon total. Coefficient RV = 0,79, $P < 0{,}0001$ après 9999 permutations.

	Singular value	*P*-value (perm.)	% total covar.	Correlation	*P*-value (perm.)
PLS1	0.00099273	< .0001	69.329	0.94041	< .0001
PLS2	0.00059625	< .0001	25.010	0.92222	< .0001

distances between AP deformed skulls and both circumferential types (C and T). The smallest distance was found between undeformed skulls and T-type skulls. When visualizing the deformed groups compared to the undeformed sample, the following characteristic shapes were observed (Fig. 2b–d): AP deformed skulls have anteroposteriorly shortened, vertically elevated and mediolaterally widened vaults; the mediolateral widening is more marked in the cranial base than in the posterior vault; the cranial base is shortened and widened; the petrous angle is more transverse (relative to the sagittal plane); the TMJ appears slightly more anterior, and the CBA is more acute than in undeformed skulls (140.6° vs. 142°). C deformed skulls exhibit conical vaults (posterosuperior elongation, mediolaterally narrowing), a narrower cranial base, a more medially and anteriorly positioned TMJ; the face is higher than in undeformed skulls, narrower and more projected (na-pr angle), which causes a slightly increased facial length; the CBA appears more obtuse, though the mean difference is small (142.5° vs. 142°); the foramen magnum is more horizontally inclined. The Toulouse-type deformation is distinct from the undeformed group by anteroposterior elongation and vertical reduction of the vault, with a mediolateral narrowing mostly noticeable in the anterior cranial base and the face, and the CBA is here more obtuse than seen in the undeformed skulls (146° vs 142°).

3.2. Patterns of covariation with the base and the masticatory apparatus

PLS 1 describes the largest direction of covariation (69%) between the base and the vault across the entire sample ($N = 51$). The correlation between the two blocks is 0.94 ($P < 0.0001$ after 9999 permutations; Table 4). As could be seen from the shape changes associated with this axis in the two blocks (Fig. 3), this reflected the shift to anteroposteriorly elongated vaults (though not mediolaterally expanded) and its association with both a reorientation of the anterior cranial base (f. caecum-sella) and an obtuse CBA. This change in angle appears mostly as the result of a decreased inclination of the sella-basion leg, while the f. caecum-sella leg remains essentially parallel, though vertically lower. The anteroposterior lengthening of the vault is also associated with a more horizontal orientation of the foramen magnum, as well as with a more transverse orientation of the petrous portion of the temporal bone. Finally, a clear narrowing of the anterior cranial base was observed on the sphenoid (greater and lesser wing). The individual scatter along this PLS1 suggests that the covariation described here mostly corresponds to shape differences between C and ND groups, while AP and T largely overlap (AP more with ND, while T more with C). The AP group exhibits a somewhat higher degree of scatter along PLS 1, and the distribution of individuals within this group, when subdivided into erect and oblique, suggests a different pattern of covariation within AP.

Table 5
Angular comparisons of within-group PLS; angles above the diagonal, *P*-values below the diagonal.
Tableau 5
Comparaisons des angles des PLS intragroupes ; angles au-dessus de la diagonale, valeurs *p* en dessous de la diagonale.

	AP	C	ND	T
AP	–	61.8	45.5	65.4
C	< 0.00001	–	70.3	43.7
ND	< 0.00001	< 0.01	–	67.5
T	< 0.001	< 0.00001	< 0.001	–

The masticatory portions of the skull clearly show covariation with the neurocranial shape, as demonstrated by the 2B PLS (Fig. 4). As the braincase shifted from an anteroposteriorly shortened and mediolaterally widened shape to a more conical and narrow shape, the palate, zygomatico-maxillary region and biglenoid width are likewise narrower, and the TMJ is projected anteriorly. The mandibular fossa has migrated superiorly. However, there appears to be no shortening of either height or length of the face, as represented in the present set of landmarks. The extremes of this shape change are represented mostly by undeformed skulls and AP (low scores), on the one hand, and by C-type deformations (high scores), on the other hand. Contrary to the covariation pattern between base and neurocranium, the AP group does not show any subdivision consistent with erect and oblique types.

3.3. Patterns of covariation within groups

Given the observed group structure in the overall PLS analysis of vault and base, the question of differential patterns of covariation between groups was examined by repeating the 2B PLS for each group separately and by comparing their respective axes of covariation.

Table 5 summarizes angular comparisons between the first PLS of each group, and confirms that the main directions of covariation are specific to each group. Thus, PLS1 in C shows the association of an anteroposteriorly elongated vault with an obtuse CBA and a more horizontally oriented foramen magnum, but no change in petrous inclination (the anterior cranial base appears narrower, based on the greater wing of the sphenoid). PLS1 in ND shows frontal flattening (possibly hinting at the presence of minimally deformed skulls), associated with a narrower anterior cranial base and a more horizontally oriented foramen magnum, but no obvious change in CBA. Finally, PLS1

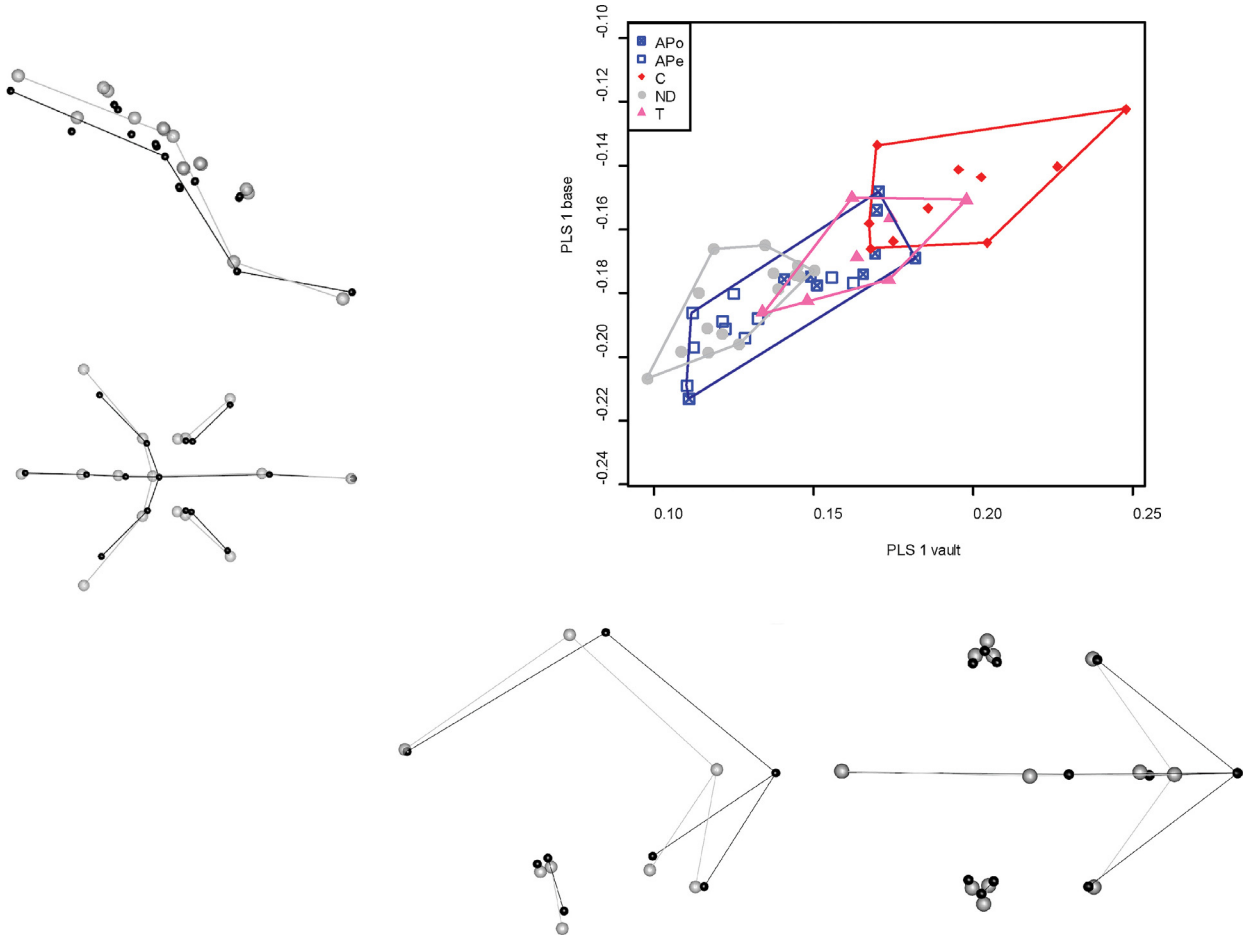

Fig. 3. Two-block partial least-squares (PLS) analysis of covariation between the vault (abscissa) and the cranial base (ordinate) (lateral and superior views). Scatterplot of individual scores for PLS 1, showing a potential subdivision into anteroposterior erect (APe, blue squares) and anteroposterior oblique (Apo, crossed out blue squares) deformations. Other symbols and colours as in Fig. 2. Shape changes associated with PLS1 in the vault and in the base. Shape changes based on regression onto PLS scores. Grey dots and lines represent low scores; high scores in black.
Fig. 3. Analyse de covariation entre la voûte (abscisse) et la base (ordonnée) par PLS en deux blocs (vues latérale et supérieure). Nuage de points des scores individuels pour PLS 1 montrant une possible subdivision entre déformation antéropostérieure verticale (APe, carrés bleus) et antéropostérieure oblique (Apo, carrés croisés bleus). Les autres symboles et couleurs sont identiques à ceux de la Fig. 2. Changements de conformation associés à PLS 1 au niveau de la voûte et de la base. Changements de conformation basés sur la régression. Les points et polygones gris représentent les valeurs minimales ; les valeurs maximales sont en noir.

in T mostly corresponds to the degree of vertical flattening and anteroposterior lengthening of the vault, which was associated with an anterior migration of the entire base, as well as basicranial flattening (within-group PLS are not displayed here).

PLS1 in AP (Fig. 5) illustrates the shift of anteroposterior compression from a lambdoid to a more nuchal position. This shift is accompanied in the base by a marked transverse reorientation of the petrous region, a posterior shift of the lesser sphenoid wing, a change from an acute to a more obtuse CBA, and by a more horizontally oriented foramen magnum. Considering the individual scores along PLS1, this pattern of covariation tends to separate the erect and oblique subtype of AP deformations. However, one oblique individual clearly deviated from this pattern. Whether this result was caused by its adolescent age, even though vault and base were nearly fully grown, remains open.

4. Discussion and conclusion

This study used 3D geometric morphometrics to investigate patterns of variation and covariation in artificially deformed skulls, particularly regarding the effects of the deformations on the base, including its masticatory elements (mandibular fossa). Previous work had mainly focused on examining how the major cranial elements develop in an integrated way under “normal” conditions (e.g., Ackermann, 2005; Bastir and Rosas, 2004; Mitteroecker and Bookstein, 2008; von Cramon-Taubadel, 2011), while the specific context of cranial deformation has largely produced 2D studies based on radiographs (but see Khonsari et al., 2013). The use of medical imaging and an explicit analysis of covariance in the present study allowed us to gain insight into the plasticity in the craniofacial region when submitted to altered growth trajectories.

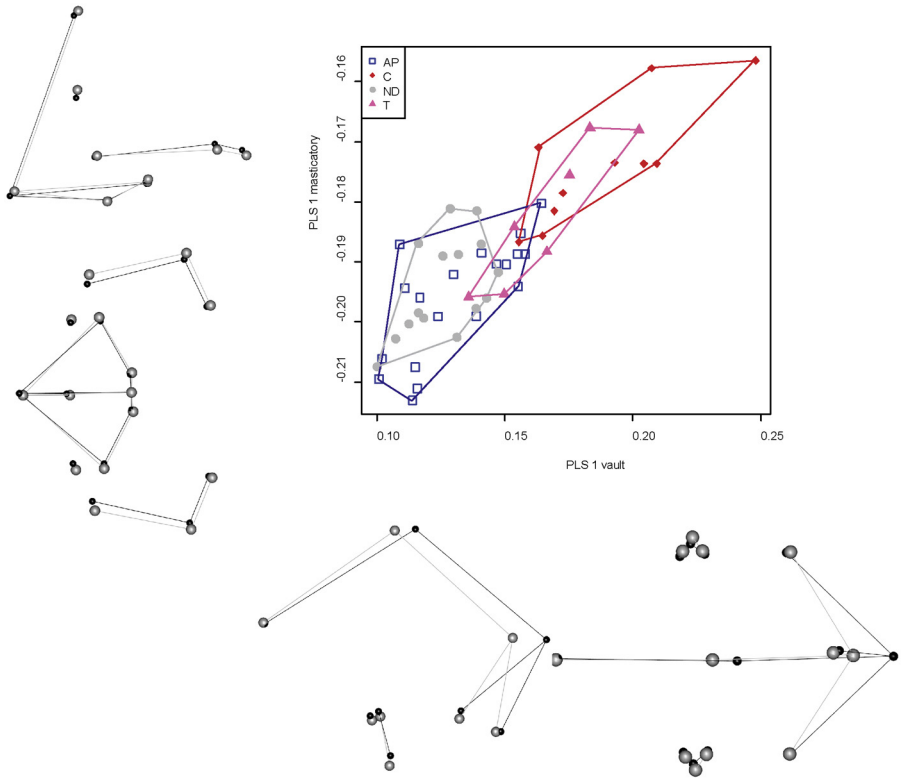

Fig. 4. Two-block partial least-squares (PLS) analysis of neurocranial (abscissa) vs. masticatory (ordinate) shapes (lateral and superior views). Scatterplot of individual scores for PLS 1. Symbols and colors as in Fig. 2. Shape changes associated with PLS1 in the vault and masticatory apparatus. Shape changes based on regression onto PLS scores. Grey dots and lines represent low scores; high scores in black.
Fig. 4. Analyse de covariation entre la voûte (abscisse) et le système masticateur (ordonnée) par PLS en deux blocs (vues latérale et supérieure). Symboles et couleurs comme sur la Fig. 2. Changements de conformation associés à PLS1 au niveau de la voûte et du système masticateur. Changements de conformation basés sur régression. Les points et polygones gris représentent les valeurs ; les valeurs maximales sont en noir.

While the sample size is still limited, making our conclusions to some degree preliminary until the findings are replicated on a larger sample, the results shed nonetheless further light on some secondary effects of cranial deformations. They confirm previous findings, according to which ACD are associated with changes in the skull base architecture, namely causing platybasia (Antón, 1989; McNeill and Newton, 1965; Oetteking, 1924), but also inducing altered proportions of the base and face (Antón, 1989; Cheverud et al., 1992; Cocilovo et al., 2011; Kohn et al., 1993; Martínez-Abadías et al., 2009). However, the notion that all deformed skulls exhibit basicranial flattening regardless of the deformation type is not corroborated by the present study. Rather, we find that AP deformed skulls, when grouped together, show a trend towards basicranial kyphosis, a finding first reported by Moss (1958; see also et al., 2009 Martínez-Abadías). We also found evidence for a more complex pattern when a possible subdivision of AP skulls into so-called “erect” and “oblique” forms is taken into consideration. Thus, our findings support the idea that AP oblique skulls conform to the general pattern of platybasia, while AP erect skulls are relatively more kyphotic, and in this respect resemble more undeformed skulls. While requiring further corroboration on a larger sample, this finding is consistent with similar results obtained on external measurements (Baylac and Friess, 2005).

The use of 3D medical imaging allowed us to also suggest specific effects of artificial deformation not really appreciable in plain X-ray films or by 3D surface data. Specifically, while narrowing of the crania base in C deformations, or shortening in AP deformations, had previously been reported (e.g., Cheverud et al., 1992; Kohn et al., 1993), our results show to which extent this affects the anterior portion. The same applies to the forward-migration of the mandibular fossa in relation to the anterior cranial base (Ferros et al., 2016), regardless of deformation type.

Previous studies of endocasts of deformed skulls have revealed modifications of craniovascular vessels, which have been interpreted as indicative of intracranial pressure changes (Dean, 1995; O’Loughlin, 1996). CT scanning could prove useful for quantifying such alterations and improve our understanding of potential clinical consequences of artificial deformation, as they cannot be observed on live subjects (Tiesler, 2014).

Interestingly, devices resembling those used to obtain ACD are used in clinical practice in order to correct posterior positional plagiocephaly, a flattening of the posterior aspect of the skull secondary to prolonged supine sleep position (Xia et al., 2008). These helmets exert lateral

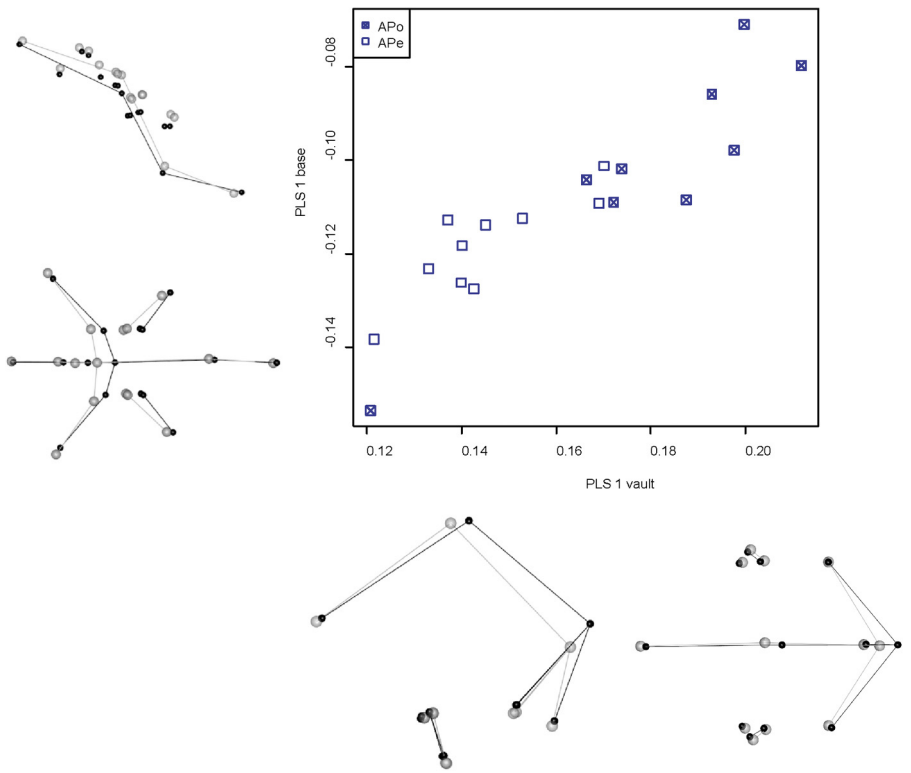

Fig. 5. Two-block partial least-squares (PLS) analysis of covariation between the vault (abscissa) and the base (ordinate) in anteroposterior (AP) deformations (lateral and superior views). Scatterplot of individual scores for PLS 1. Blue squares represent anteroposterior erect (APe) deformations, crossed out blue squares correspond to the anteroposterior oblique type (APo). Shape changes associated with PLS1 in the vault and base. Shape changes based on regression onto PLS scores. Grey dots and lines represent low scores; high scores are in black.

Fig. 5. Analyse de covariation entre la voûte (abscisse) et la base des crânes (ordonnée) ayant subi une déformation antéropostérieure (AP) par PLS en deux blocs (vues latérale et supérieure). Changements de conformation associés à PLS1 aux niveaux de la voûte et de la base. Changements de conformation basés sur régression. Les points et polygones gris représentent les valeurs minimales ; les valeurs maximales sont en noir.

pressure on the skull vault, as they are designed to fight against excessive anteroposterior flattening. The assessment of the influence, if any, of helmet therapy on basicranial flattening would be of tremendous interest in the discussion of the differential influence of AP and C deformations on craniofacial structures, as it would exhibit the effects of forces perpendicular to both usual ACD modalities.

Several other patterns of cranial alteration add further weight to the hypothesis that differences in deformation techniques lead to different responses of the growing skull: (1) the anterosuperior shift of the mandibular fossa, part of the temporomandibular joint; (2) the sagittal reorientation of the petrous region in AP skulls, particularly in the erect subtype; and (3) the more horizontally inclined foramen magnum in C deformations, in conjunction with the significant differences in the angles of the first PLS axes between groups, illustrate that the vault, base and masticatory portions of the skull function as integrated structures. These results stress the plasticity with which the human cranium reacts to mechanical constraints during growth along different trajectories and in direct response to the nature of the deformation device.

The modification in the position of the mandibular fossa in different ACDs is of particular importance for the understanding of induced growth alterations of the craniofacial region, as an anterior shift of the mandibular fossa is a known factor in the development of dento-skeletal anomalies where the lower jaw is shifted forward. These anomalies can lead to class III malocclusion, depending on the maxillary and dental compensations for the abnormal mandibular position (Delaire et al., 1981).

Present results thus indicate that abnormal constraints exerted on the skull vault can have an influence on the position on the mandible, and thus on occlusion, via modifications in the position of the mandibular fossa of the skull base. Nevertheless, several studies devoted to the structure of the mandible in ACDs indicate that vault deformations do not induce occlusal anomalies, despite significant modifications in the shape of the mandible (Cheverud and Midkiff, 1992; Ferros et al., 2016; Jimenez et al., 2012). The absence of malocclusion in ACD most probably corresponds to compensatory mechanisms that could be better understood by 3D studies of the shape of the lower jaw, as currently available studies on the mandible have been performed using 2D data. Furthermore, studying occlusion in dry skulls relies on an approximate placement of the condylar head into the mandibular fossa, without taking into account the soft tissues forming the temporomandibular joint.

In sum, current data on the mandible in ACDs (Ferros et al., 2016) suggest that potential occlusal anomalies (class III malocclusion) – that could be predicted by the anterior displacement of the mandibular fossa – are compensated by mechanisms most probably involving 3D mandibular shape modifications. A simple way to progress in the understanding of these compensatory mechanisms would be to assess the 3D angulation of the occlusal plane, but this again relies on an appropriate positioning of the condylar heads relative to the skull base, and therefore renders the inclusion of the mandible a not so trivial issue when working with dry skulls.

As a whole, we provided support for differential effects of different types of ACD on craniofacial growth, and our results may be seen as further indication of the existence of multiple cranial modules, such as the petroso-mandibular unit (Bastir and Rosas, 2004, 2005; Bastir et al., 2004), though testing modularity hypotheses is beyond the scope of this study and should be addressed in future research on ACD.

Our findings also lend support to the idea that the basic dichotomy of AP vs. C deformations does not well represent the shape variation (e.g., Manríquez et al., 2006), at least with respect to internal structures. Future work should focus on classifying ACD in a manner consistent with both ethnographic data on devices, as well as with the resulting internal and external shape (co)variation. Improved classifications may benefit from the use of semilandmarks (e.g., Perez, 2007). As indicated above, the cranial vault is not extensively covered by standard landmarks, so that it is conceivable that minute shape variations that may help in the classification process are not well accounted for here. After all, the tremendous amount of shape variation seen in deformed crania around the world is a direct reflection of the diversity of cultural practices responsible for the morphological variability, and any classification system is prone to reductionist fallacies.

Acknowledgements

We are grateful to Aurélie Fort, Véronique Laborde and Liliana Huet for their assistance in accessing collections at MNHN. We thank three anonymous reviewers and the Associate Editor for their valuable comments and advice that helped improve this manuscript. We are thankful to Roberto Macchiarelli for inviting us to this constribution. We wish to acknowledge MH@SU and Pascal Frey (Chaire Facile, Sorbonne Université) for financial support.

This is an invited paper to the thematic issue of *Comptes rendus Palevol* entitled "Hominin biomechanics, virtual anatomy and inner structural morphology: From head to toe. A tribute to Laurent Puymerail", edited by R. Macchiarelli and C. Zanolli. MF dedicates this contribution to the memory of Laurent, who inspired so many in so few years.

References

Adams, D.C., Otarola-Castillo, E., 2013. Geomorph: an R package for the collection and analysis of geometric morphometric shape data. Methods Ecol. Evol. 4, 393–399.

Ackermann, R.R., 2005. Ontogenetic integration of the hominoid face. J. Hum. Evol. 48, 175–197.

Antón, S.C., 1989. Intentional cranial vault deformation and induced changes of the cranial base and face. Am. J. Phys. Anthropol. 79, 253–267.

Antón, S.C., Weinstein, K.W., 1999. Artificial cranial deformation and fossil Australians revisited. J. Hum. Evol. 36, 195–209.

Badawi-Fayad, J., Yazbeck, C., Balzeau, A., Nguyen, T.H., Istoc, A., Grimaud-Hervé, D., Cabanis, E.A.M., 2005. Multi-detector row CT scanning in paleoanthropology at various tube current settings and scanning mode. Surg. Radiol. Anat. 7, 1–8.

Bastir, M., Rosas, A., 2004. Facial heights: Evolutionary relevance of postnatal ontogeny for facial orientation and skull morphology in humans and chimpanzees. J. Hum. Evol. 47, 359–381.

Bastir, M., Rosas, A., 2005. Hierarchical nature of morphological integration and modularity in the human posterior face. Am. J. Phys. Anthropol. 128, 26–34.

Bastir, M., Rosas, A., Kuroe, K., 2004. Petrosal orientation and mandibular ramus breadth: Evidence for an integrated petroso-mandibular developmental unit. Am. J. Phys. Anthropol. 123, 340–350.

Baylac, M., Friess, M., 2005. Combining Procrustes Superimposition and Fourier descriptors: Analysis of midsagittal cranial outlines. In: Slice, D.E. (Ed.), Modern Morphometrics in Physical Anthropology. Kluwer, New York, pp. 145–165.

Bookstein, F.L., Gunz, P., Mitteroecker, P., Prossinger, H., Schaefer, K., Seidler, H., 2003. Cranial integration in *Homo*: Singular warps analysis of the midsagittal plane in ontogeny and evolution. J. Hum. Evol. 44, 167–187.

Bräuer, G., 1988. Osteometrie. In: Knussmann, R., Martin, R. (Eds.), Anthropologie: Handbuch der vergleichenden Biologie des Menschen, Band 1. Gustav Fischer Verlag, Stuttgart, pp. 160–231.

Broca, P., 1871. Sur la déformation artificielle de la tête dans la région toulousaine. Bull. Mém. Soc. Anthropol. Paris 6, 100–131.

Brown, P., 1981. Artificial cranial deformation: A component in the variation in Pleistocene Australian Aboriginal crania. Archaeol. Oceania 16, 156–167.

Buikstra, J.E., Ubelaker, D.H., 1994. Standards for Data Collection from Human Skeletal Remains. Arkansas Archaeological Survey Research Series 44. Fayetteville, Arkansas.

Chervin, A., 1908. Anthropologie Bolivienne. In: Tome III : Craniologie. Imprimerie nationale, Paris.

Cheverud, J.M., Kohn, L.A.P., Konigsberg, L.W., Leigh, S.R., 1992. Effects of fronto-occipital artificial cranial vault modification on the cranial base and face. Am. J. Phys. Anthropol. 88, 323–345.

Cheverud, J.M., Midkiff, J.E., 1992. Effects of fronto-occipital cranial reshaping on mandibular form. Am. J. Phys. Anthropol. 87, 167–171.

Clark, J., Dobson, L.S.D., Antón, S.C., Hawks, J., Hunley, K.L., Wolpoff, M.H., 2007. Identifying artificially deformed crania. Int. J. Osteroarcheol. 17, 596–697.

Cocilovo, J.A., Varela, H.H., O'Brien, T.G., 2011. Effects of artificial deformation on cranial morphogenesis in the South Central Andes. Int. J. Osteoarchaeol. 21, 300–312.

Couette, S., White, J., 2010. 3D geometric morphometrics and missing data. Can extant taxa give clues for the analysis of fossils primates? C. R. Palevol 9, 423–433.

Créqui Monfort, G., Sénéchal de La Grange, E., 1904. Rapport sur une Mission Scientifique en Amérique du Sud (Bolivie, République Argentine, Chili, Pérou). Imprimerie nationale, Paris.

Dean, V.L., 1995. Sinus and meningeal vessel pattern changes induced by artificial cranial deformation: A pilot study. Int. J. Osteoarchaeol. 5, 1–14.

Delaire, J., Schendel, S.A., Tulasne, J.F., 1981. An architectural and structural craniofacial analysis: A new lateral cephalometric analysis. Oral Surg. Oral Med. Oral Pathol. 52, 226–238.

Dembo, A., Imbelloni, J., 1938. Deformaciones Intencionales del Cuerpo Humano de Carácter Etnico. Editori Nova, Buenos Aires.

Dingwall, E.J., 1931. Artificial Cranial Deformation. A Contribution to the Study of Ethnic Mutilations. J. Bale, Sons & Danielsson, Ltd, London.

Dryden, I.L., 2015. Shapes package. R Foundation for Statistical Computing, Vienna, Austria. Contributed package (Version 1.1–11. URL http://www.R-project.org).

Fajardo, R.J., Ryan, T.M., Kappelman, J., 2002. Assessing the accuracy of high-resolution X-ray computed tomography of primate trabecular bone by comparisons with histological sections. Am. J. Phys. Anthropol. 118, 1–10.

Falkenburger, F., 1938. Recherches anthropologiques sur la déformation artificielle du crâne. J. Soc. Am. Paris 30, 1–70.

Ferros, I., Mora, M.J., Obeso, I.F., Jimenez, P., Martinez-Insua, A., 2016. Relationship between the cranial base and the mandible in artificially deformed skulls. Orthod. Craniofac. Res. 19, 222–233.
Friess, M., Baylac, M., 2003. Exploring artificial cranial deformation using Elliptic Fourier Analysis of Procrustes aligned outlines. Am. J. Phys. Anthropol. 122, 11–22.
Hoshower, L.M., Buikstra, J.E., Goldstein, P.S., Webster, A.D., 1995. Artificial cranial deformation at the Omo M10 site: A Tiwanaku complex from the Moquegua Valley. Peru. Lat. Am. Antiq. 6, 145–164.
Janusek, J.W., 2008. Ancient Tiwanaku. Cambridge University Press, Cambridge.
Jimenez, P., Martinez-Insua, A., Franco-Vazquez, J., Otero-Cepeda, X.L., Santana, U., 2012. Maxillary changes and occlusal traits in crania with fronto-occipital deformation. Am. J. Phys. Anthropol. 147, 40–51.
Khonsari, R.H., Friess, M., Nysjö, J., Odri, G., Malmberg, F., Nyström, I., Messo, E., Hirsch, J.M., Cabanis, E.A., Kunzelmann, K.H., Salagnac, J.M., Corre, P., Ohazama, A., Sharpe, P.T., Charlier, P., Olszewski, R., 2013. Shape and volume of craniofacial cavities in intentional skull deformations. Am. J. Phys. Anthropol. 151, 110–119.
Klingenberg, C.P., 2011. MorphoJ: An integrated software package for geometric morphometrics. Molec. Ecol. Resour. 11, 353–357.
Klingenberg, C.P., Marugán-Lobón, J., 2013. Evolutionary covariation in Geometric Morphometric data: Analyzing integration, modularity, and allometry in a phylogenetic context. Syst. Biol. 62, 591–610.
Klingenberg, C.P., Zimmermann, M., 1992. Static, ontogenetic, and evolutionary allometry: A multivariate comparisons in nine species of water striders. Am. Nat. 140, 601–620.
Kohn, L.A.P., Leigh, S.R., Jacobs, S.C., Cheverud, J.M., 1993. Effects of annular cranial vault modification on the cranial base and face. Am. J. Phys. Anthropol. 90, 147–168.
Liebermann, D.E., Pearson, O.M., Mowbray, K.M., 2000. Basicranial influence on overall cranial shape. J. Hum. Evol. 38, 291–315.
Manouvrier, L., De Mortillet, A., 1893. Collection préhistorique du Dr Prunières. Bull. Soc. Anthropol. Paris 4 (4e série), pp. 352–364.
Manríquez, G., González-Bergás, F.E., Salinas, J.C., Espoueys, O., 2006. Deformación intencional del cráneo en poblaciones arqueológicas de Arica, Chile: análisis preliminar de morfometría geométrica con uso de radiografías craneofaciales. Chungará 38, 13–34.
Martínez-Abadías, N., Paschetta, C., de Azevedo, S., Gonzalez-José, R., 2009. Developmental and genetic constraints on neurocranial globularity: Insights from analyses of deformed skulls and quantitative genetics. Evol. Biol. 36, 37–56.
McNeill, R.W., Newton, G.N., 1965. Cranial base morphology in association with intentional cranial vault deformation. Am. J. Phys. Anthropol. 23, 241–254.
Mitteroecker, P., Bookstein, F.L., 2008. The evolutionary role of modularity and integration in the hominoid cranium. Evolution 62, 943–958.
Moss, J.L., 1958. The pathogenesis of artificial cranial deformation. Am. J. Phys. Anthropol. 16, 269–286.
O'Brien, T.G., Stanley, A.M., 2011. Boards and cords: Discriminating types of artificial cranial deformation in prehispanic South Central Andean populations. Int. J. Osteoarch. 23, 459–470.
Oetteking, B., 1924. Declination of the pars basilaris in normal and in artificially deformed skulls. A study based on the skulls of the Chumash of San Miguel Island, California, and on those of the Chinook. Indian Notes Monogr. 27, 3–25.
O'Loughlin, V.D., 1996. Comparative endocranial vascular changes due to craniosynostosis and artificial cranial deformation. Am. J. Phys. Anthropol. 101, 369–385.
Perez, S.I., 2007. Artificial cranial deformation in South America: A geometric morphometrics approximation. J. Archaeol. Sci. 34, 1649–1658.
R Development Core Team, 2016. R: A Language and Environment for Statistical Computing. Version 3.30. R Foundation for Statistical Computing, Vienna.
Rohlf, F.J., 2000. Statistical power comparisons among alternative morphometric methods. Am. J. Phys. Anthropol. 111, 463–478.
Rohlf, F.J., Corti, M., 2000. Use of two-block partial least-squares to study covariation in shape. Syst. Biol. 49, 740–753.
Schendel, S.A., Walker, G., Kamisugi, A., 1980. Hawaiian cranial morphometrics: Average Mokapuan skull, artificial cranial deformation, and the "rocker" mandible. Am. J. Phys. Anthropol. 52, 491–500.
Schlager, S., 2016. Morpho: Calculations and Visualizations Related to Geometric Morphometrics. R package version 0.21 (Available at: http://sourceforge.net/project/morpho-rpackage/).
Spoor, C.F., Zonneveld, F.W., Macho, G.A., 1993. Linear measurements of cortical bone and dental enamel by computed tomography: applications and problems. Am. J. Phys. Anthropol. 91, 469–484.
Tiesler, V., 2014. The Bioarchaeology of Artificial Cranial Deformations. New Approaches to Head Shaping and its Meanings in Pre-Columbian Mesoamerica and Beyond. Springer, New York.
Torres-Rouff, C., 2002. Cranial vault modification and ethnicity in middle horizon San Pedro de Atacama, Chile. Curr. Anthropol. 43, 163–171.
Verano, J.W., 2003. Human skeletal remains from Machu Picchu: A reexamination of the Yale Peabody Museum's Collections. In: Burger, R.L., Salazar, L.C. (Eds.), The 1912 Yale Peruvian Scientific expedition Collections from Machu Picchu. Human and Animal Remains, 85. Yale University Publications in Anthropology, pp. 65–117.
von Cramon-Taubadel, N., 2011. The relative efficacy of functional and developmental cranial modules for reconstructing global human population history. Am. J. Phys. Anthropol. 146, 83–93.
Xia, J.J., Kennedy, K.A., Teichgraeber, J.F., Wu, K.Q., Baumgartner, J.B., Gateno, J., 2008. Nonsurgical treatment of deformational plagiocephaly: A systematic review. Arch. Pediatr. Adolesc. Med. 162, 719–727.